POLITECNICO DI TORINO
Repository ISTITUZIONALE

Investigation on the Static Characteristics of a Dynamic Gas Thrust Bearing with Spiral Grooves for a Small-Scale High-Speed Application

Original
Investigation on the Static Characteristics of a Dynamic Gas Thrust Bearing with Spiral Grooves for a Small-Scale High-Speed Application / Colombo, F., Goti, E., Lentini, L., Raparelli, T.. - 160:(2024), pp. 180-190. (5th International Tribology Symposium of IFToMM, ITS-IFToMM 2024 Salerno (IT) May 6th-8th, 2024) [10.1007/978-3-031-62616-6_19].

Availability:
This version is available at: 11583/2995529 since: 2026-03-23T09:55:49Z

Publisher:
Springer Science and Business Media

Published
DOI:10.1007/978-3-031-62616-6_19

Terms of use:

This article is made available under terms and conditions as specified in the corresponding bibliographic description in the repository

Publisher copyright
Springer postprint/Author's Accepted Manuscript (book chapters)

This is a post-peer-review, pre-copyedit version of a book chapter published in Proceedings of ITS-IFToMM 2024. The final authenticated version is available online at: http://dx.doi.org/10.1007/978-3-031-62616-6_19

(Article begins on next page)

19 November 2026

Investigation on the static characteristics of a dynamic gas thrust bearing with spiral grooves for a small-scale high-speed application

Federico Colombo[1[0000-0002-1054-236X]], Edoardo Goti[1[0000-0002-1352-6410]], Luigi Lentini[1[0000-0003-3770-3773]] and Terenziano Raparelli[1[0000-0003-0063-7733]]

[1] Politecnico di Torino, Department of Mechanical and Aerospace Engineering, Torino, Italy
federico.colombo@polito.it

Abstract. This paper focuses on the design of a spiral groove thrust bearing for a high-speed, small-scale radial compressor rotating at 200 krpm. The analytical model from Muijderman is taken into account to estimate the load carrying capacity and the stiffness of the thrust bearing. In this preliminary study, the static analysis is carried out in order to design the geometry of the bearing, which is of spiral groove type. The outer and inner diameter of the thrust bearings are 30 mm and 17 mm respectively. After a short recall of the literature model, the geometry of the bearing is optimized in order to maximize its load capacity. Future investigations will be aimed at evaluating the bearing stability in dynamic conditions. The experimental validation of the model is also forecast.

Keywords: dynamic gas bearings, narrow-groove theory, lubrication, thrust bearings, spiral grooved bearings

Nomenclature

α: inclination angle
$\delta=h_2/h_0$: groove height ratio
$\gamma = a_2/a_1$: ridge to groove width ratio
μ: viscosity of air
$\Gamma=r_b/r_2$: radius ratio
ρ: air density
ω: rotational speed (rad/s)
$a_1(r)$: width of groove
$a_2(r)$: width of ridge
b: radial length of grooved part
c: radial length of ungrooved part
h_0: groove depth
h_1: film clearance in the groove
h_2: film clearance in the ridge
$H=h_2/h_1$: film height ratio
k: number of grooves
n: rotational speed (rpm)
p_0: ambient pressure
r_1: inner radius
r_2: outer radius
r_b: end-of-groove radius
s^*: radial mass flow for one groove and one ridge
s_t: total radial mass flow
S: flow parameter
W: load capacity

Introduction

Dynamic gas bearings have special properties that make them suitable for high-speed mobile applications. First of all, they do not need an auxiliary system for the air compression, as the pressure distribution that creates the load carrying capacity is generated by the rotation itself. Secondly, the absence of sliding contacts makes them suitable for high-efficiency systems, as the losses in bearings are minimized.

A peculiar type of dynamic air bearing is the grooved bearing, whose surface is endowed of some grooves of proper geometry, so as to create the air pumping action inside the bearing during rotation. These are employed in high-speed turbomachines of small scale; for example, for heat pumps [1], fuel cell blowers [2] or recirculation devices [3]. In [4] it is demonstrated the feasibility of a twin-stage radial flow compressor with impellers of diameter about 19 mm rotating at 250 krpm and total shaft power of 6 kW for domestic heat pump application. The advantage of this small-scale radial compressor is the higher coefficient of performance and higher efficiency that it is possible to attain with respect to conventional volumetric compressors. A review is given in [5], showing the applicability of gas bearings with compliant elements for high-speed oil free air cycle machines. Walton et al. [6] describe applications to cryogenic devices, in which the cryogenic fluid is employed as a lubricant for the supports. Among the different types of dynamic gas bearings, grooved bearings are appreciated for their compactness and simplicity in manufacturing.

Whipple [7] firstly developed an analytical model for the estimation of the load capacity of grooved thrust bearings. Muijderman [8] further developed this model introducing the effect of curvature of grooves. Such models are part of the so-called Narrow Groove Theory (NGT), which assumes an infinite number of grooves in order to neglect the pressure variation across the groove/ridge couple and simplify the analysis. It is so possible to obtain an analytical expression for the load capacity as a function of the thrust bearing geometry.

Different contributions to the NGT have been proposed over the years. This theory was first extended to journal bearings in [9] and experimentally validated in [10, 11]. An overview of the state-of-the-art on grooved bearings can be found in [12] where insights about modeling and design guidelines are given.

There exist alternative approaches to the NGT, which involve the discretization of the fluid film and the solution of the Reynolds equation. Such approaches can involve the finite difference methods [13] or the finite element method [14]. The static and dynamic coefficients of spiral-grooved gas journal bearings are obtained in [15], while the NGT is also extended to configurations of interests in seals [16]. A spiral grooved thrust bearing is investigated with CFD technique in case of uncompressible lubricant fluid in [17]. A different geometry is simulated in [18]; it consists of a spiral-grooved opposed-hemisphere double gas bearing.

In this paper, the model from [8] is employed for the design of a thrust bearing of spiral type, partially grooved and with inwardly pumping. The paper is also aimed at evaluating the curvature effect introduced by the model and compare it with model [7], which does not take this effect into account.

The literature model

The groove patterns for thrust bearings can be with inward, outward or both effects configurations [19, 20]. The geometry of the thrust bearing investigated in this paper is depicted in Fig. 1. Inward configuration is considered in this work (with clockwise rotation) since the pump-in design of SGTB was confirmed to guarantee superior load carrying capacity compared to the other designs [21]. A series of spiral shaped grooves is presented on the rotating thrust surface. The grooved surface is not complete, as the innermost part of the bearing is ungrooved. The rotation involves a pumping effect that creates a pressure gradient in the radial direction, with a maximum mean pressure at the end-of-groove radius r_b. The grooves are inclined of angle α measured w.r.t. the circumferential direction. The grooves and the ridges widths along the circumferential direction are a_1 and a_2. Due to the spiral shape, such widths are variable with the radius.

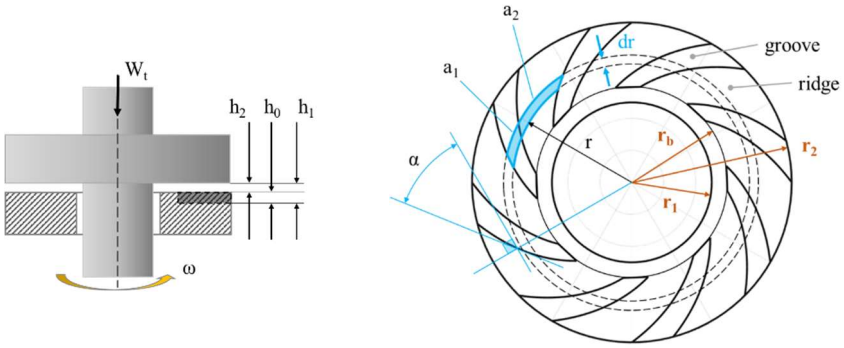


Fig. 1. Sketch of the spiral grooved geometry; the blue-shaded region represents the basic element dp_r of equation (1) is calculated for.

The model from [8] is taken into account for the estimation of the load capacity and stiffness of the thrust bearing. Each basic element, located at radius r (see figure 1), contributes to create the pressure gradient along the radial direction. The expression of the pressure built-up due to the element is:

$$-\mathrm{d}p_r = -\frac{6\mu\omega r}{h_2^2} H^2 \frac{num_1 + S \cdot num_2}{den} dr \tag{1}$$

where

$$num_1 = \gamma(1-H)\cot\alpha\,(-1+H^3) \tag{2}$$

$$num_2 = (\gamma + H^3)(\cot^2\alpha + 1) \tag{3}$$

$$den = (1+\gamma H^3)(\gamma + H^3) + H^3\cot^2\alpha\,(1+\gamma)^2 \tag{4}$$

S is the dimensionless leakage flow through fields 1 and 2 in radial direction:

$$S = \frac{2s^*}{\omega r h_1 a_1 \rho_0} \tag{5}$$

and s^* the mass flow which crosses one groove and one ridge along the radial direction.

The width of the groove at radius r is given by equation (6)

$$a_1(r) = \frac{2\pi r}{k(1+\gamma)} \tag{6}$$

where k is the number of grooves and $\gamma = a_2/a_1$ the ridge to groove width ratio, which is constant along the radial direction. The total radial flow is $s_t = k \cdot s^*$. Note that, despite k explicitly defines $a_1(r)$, this model remains insensitive to the number of grooves since $\mathrm{d}p_r$ is function of γ only.

Considering as boundary conditions ambient pressure at the inner and outer radius, the pressure build-up in the basic element can be integrated along the radial direction in order to calculate the overall built-up pressure:

$$p_{rb} - p_0 = -\int_{r_b}^{r_2} \mathrm{d}p_r \tag{7}$$

while the generic pressure at radius r is

$$p(r) = p_r = p_0 - \int_{r}^{r_2} \mathrm{d}p_r \tag{8}$$

The load carrying capacity of the grooved part is then obtained by integrating along the radius the pressure built-up in the basic element:

$$W_{gr} = \int_{r_b}^{r_2} 2\pi r (p_r - p_0)\, dr \tag{9}$$

In the ungrooved part of the thrust bearing the pressure distribution is logarithmic:

$$p_r = p_0 + (p_{rb} - p_0)\frac{\ln r - \ln r_1}{\ln r_b - \ln r_1} \tag{10}$$

and the load capacity of the ungrooved part is

$$W_{ungr} = \int_{r_1}^{r_b} 2\pi r (p_r - p_0)\, dr \tag{11}$$

As the radial flow in the ungrooved part must coincide with the flow in the grooved part, equation (12) holds

$$s_t = s^* k = \frac{\pi \rho_0 h_2^3 (p_{rb} - p_0)}{6\mu \ln r_b / r_1} \tag{12}$$

where the right-hand side expression represents the flow in the ungrooved region.

This relationship can be used to couple the pressure distribution in the two regions and solve the problem. Equation 1 is solved for Δp_r once equation 12 and 5 are substituted into it. The pressure built-up across the basic element is then integrated to obtain the total load capacity of the bearing through equation 9 and 11. Figure 2 sketches the algorithm used to calculate the load capacity through the evaluation of pressure p_{rb}.

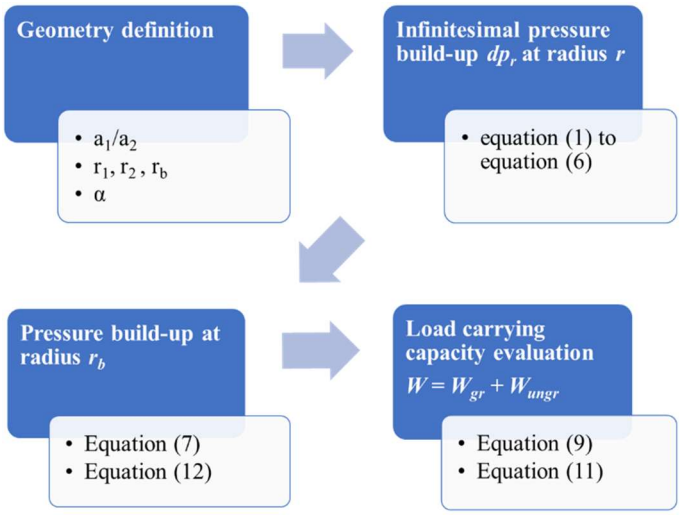


Fig. 2. Sketch of the algorithm employed for the calculation of the load capacity of the thrust bearing.

Reference geometry and characteristic stiffness curve

For the design of the thrust bearing of our application, the following geometrical parameters were fixed: outer radius r_2=15 mm, inner radius r_1=8.5 mm, film height h_2=10 μm. On the contrary, the design parameters are: groove angle α, ridge to groove width ratio γ, end of groove radius to outer radius ratio Γ, groove depth to film height ratio δ. The number of grooves is not taken into account by the model as the main assumption is to suppose an infinite number of grooves.

A reference geometry is considered to study the variation of the load capacity with respect to the film height h_2 which provides also a measure of the axial stiffness of the thrust bearing. The reference geometry is defined by the following values:

$$\alpha = 45°$$
$$\gamma = a_2/a_1 = 1$$
$$\Gamma = r_b/r_2 = 0.7$$
$$\delta = h_2/h_0 = 0.6$$

The film height in the ridge is varied in the range from 3 to 16 μm. Fig. 3 shows the load capacity versus film height curve, together with the stiffness curve, i.e., its first derivative. Two rotating speed values are considered: 100 krpm and 200 krpm. The figure shows that in both cases the stiffness characteristic is highly non-linear, and high stiffening is expected below 6 μm of film thickness.

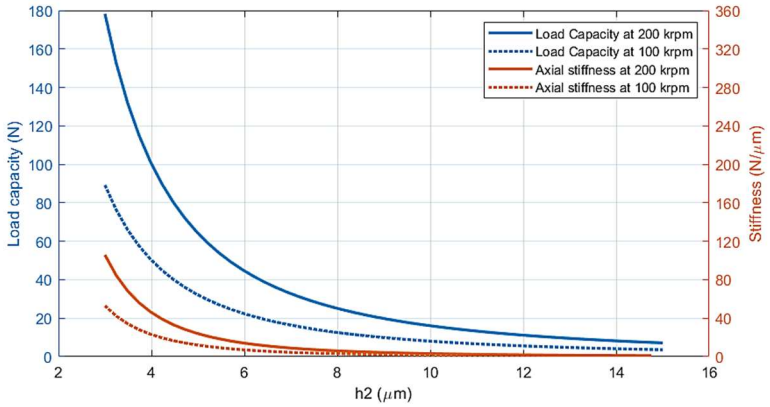


Fig. 3. Load capacity and stiffness curve of the bearing vs film height h_2.

Sensitivity analysis

In order to perform the sensitivity analysis of the model and evaluate the influence of each parameter, the design parameters are changed (one at a time) within the following ranges:

$$10° < \alpha < 70°$$
$$0.2 < \gamma < 2$$
$$0.6 < \Gamma < 0.9$$
$$0.2 < \delta < 1$$

The results related to a fixed rotational speed equal to n = 200 krpm are shown in Figs. 4 and 5 in terms of the overall load capacity, i.e. the sum of the load capacity provided by the grooved and ungrooved part of the bearing. The film thickness h_2 is equal to 10 μm like in the reference geometry.

From the sensitivity analysis it emerges that angle α must be large enough to have an appreciable radial pumping effect in the grooves, entailing an appreciable load carrying capacity of the bearing (figure 4, left). The maximum load capacity corresponds to $\alpha \approx 28°$. Similarly, it is useless to increase this angle beyond 40° as the sliding speed component along the groove reduces too much, entailing a decrease in the load capacity. The ridge-to-groove ratio γ is to be chosen in range $0.5 < \gamma < 1$ (figure 4, right) where its influence is quite negligible; this means that the groove width must be bigger than the ridge width ($a_1 > a_2$) but not too big ($a_1 < 2a_2$). In case the ridge is too small, the load capacity decreases again with respect to the optimum as there is not enough ridge surface for the flow to leaks from the center of the bearing outwards. The base radius r_b at which the groove ends must be approx. 0.7 times the external radius r_2 (figure 5, left). The film thickness h_2 must be approximately half the groove depth h_0 in order to have the maximum load capacity (figure 5, right). Regarding the choice of parameters Γ and δ, they are already close to optimality in the reference geometry, as the local maximum of the load capacity corresponds to $\Gamma \approx 0.7$ and $\delta \approx 0.6$ (see section on optimization).

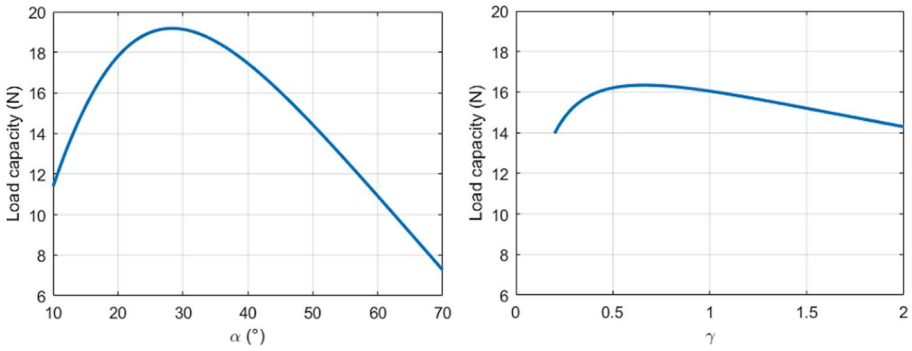


Fig. 4. Load capacity of the thrust bearing vs groove angle α (left) and vs γ (right).

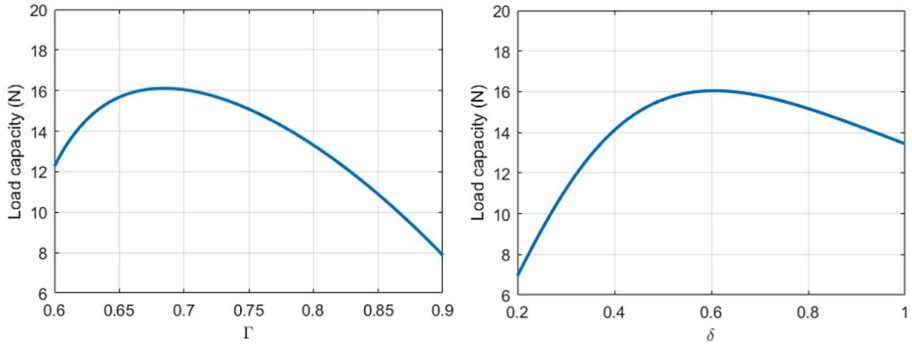


Fig. 5. Load capacity of the thrust bearing vs Γ (left) and vs δ (right).

Comparison with another literature model

In this section, the results provided by the Muijderman model are compared with the results from the previous model by Whipple [7], in which the effect of curvature is not taken into account. The reference geometry described in the previous section is investigated with both models [7] and [8]. The load capacity per unit length and the flow per unit length through the bearing are compared in Fig. 6 and Fig. 7. Because of curvature, the load capacity per unit length and the flow per unit length are affected by the radial distance from the rotation axis. The average radius r_m of the grooved regions is considered for this comparison, as per equation 13.

$$r_m = \frac{r_b + r_2}{2} \tag{13}$$

The Whipple model neglects the effect of curvature, i.e. this model is strictly valid for an ideal linear thrust bearing, where the sliding speed, which is responsible of the pumping action, is constant all over the thrust surface. The model from Muijderman, on the contrary, estimates the contribution to the pressure gradient with a weight proportional to the radius, as from eq. (1). In this case, the comparison with the Muijderman

model is possible under the hypothesis that at any radius the tangential speed is equal to u_m, i.e., the tangential speed at the average radius r_m of the grooved region.

$$u_m = \omega \cdot r_m \tag{14}$$

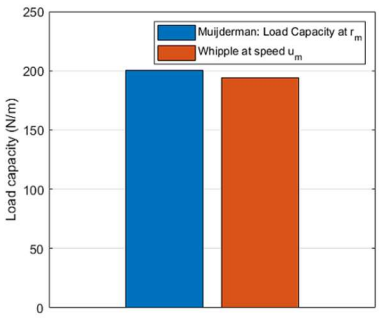


Fig. 6. Comparison between the load capacity calculated through the Muijderman model and that from Whipple.

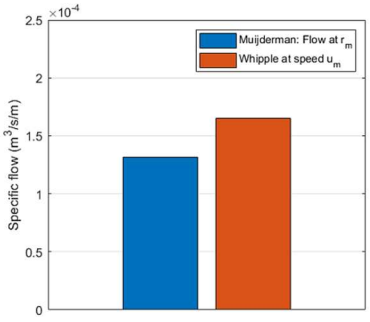


Fig. 7. Comparison between the specific radial flow calculated through the Muijderman model and that from Whipple.

The load capacity calculated according to Whipple's model is 3% lower of that calculated through the one by Muijderman. As to the flow per unit length, Whipple's model provides a value that is 25% higher compared to Muijderman's model. These two results are in line with the NGT since the maximum load capacity of a spiral groove bearing is achieved when the flow velocity at the inner groove tip is null. In summary, the curvature of the spirals has an effect on the pressure build-up, although negligible at least in the given configuration considered in this analysis. Regarding the estimation of the radial flow, the curvature effect is more important and cannot be neglected.

Optimization

The optimization of the geometry of the bearing is carried out considering a film thickness h_2 equal to 10 μm and speed ω=200 krpm. The optimal set of design parameters is searched in the same range already considered for the sensitivity analysis with the aim of maximizing W. A goal-seeking algorithm was exploited that looks for the values α, γ, Γ, and δ at which the load capacity reaches its highest value $\overline{W}$.

The outcome of the geometry optimization process is provided in Table 1 and represented in Figure 8.

Table 1. Optimized design parameters

α	γ	Γ	δ	$\overline{W}$
17.5°	0.617	0.684	0.330	22 N

The maximum load capacity obtained at 200 krpm is about 22 N. Interestingly, the optimization of the bearing design is insensitive to speed and film thickness variation, which means that high efficiency is also obtained in off-design operation.

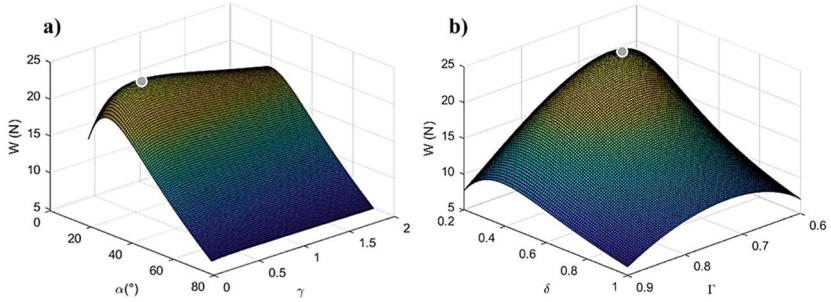


Fig. 8. Optimized load capacity (a) versus α and γ; (b) versus Γ and δ.

Conclusions

A spiral groove thrust bearing is designed using a literature analytical model. A comparison between two models is given to evaluate the accuracy of the simplified model in estimating the load capacity. The comparison reveals that the two models are in a good accordance in estimating the load carrying capacity of the thrust bearing in the reference geometry. The effect of the groove curvature which is considered in the Muijderman's model and neglected in the Whipple's one is limited, especially as regard the estimation of the load carrying capacity.

The sensitivity analysis reveals the effect of each design parameter while optimization of these parameters allowed to find the geometry that maximizes the load capacity for the application of interest.

In the future, the aim of the authors is to compare the results of these analytical models with FE models where the fluid-structure interaction is simulated and validate the models with experimental data measured with a real prototype.

Acknowledgments

This publication is part of the project NODES which has received funding from the MUR – M4C2 1.5 of PNRR funded by the European Union - NextGenerationEU (Grant agreement no. ECS00000036)

References

1. Schiffmann, J. and Favrat, D. (2010), "Integrated Design and Optimization of Gas Bearing Supported Rotors," Journal of Mechanical Design, 132(5), pp 051007.
2. Schiffmann, J. (2015), "Integrated Design and Multi-Objective Optimization of a Single Stage Heat-Pump Turbocompressor," Journal of Turbomachinery, 137(7), pp 071002.

3. Wagner, P. H., Wuillemin, Z., Diethelm, S., Van Herle, J., and Schiffmann, J. (2017), "Modeling and Designing of a Radial Anode Off-Gas Recirculation Fan for Solid Oxide Fuel Cell Systems," Journal of Electrochemical Energy Conversion and Storage, 14(1), pp 011005.
4. Schiffmann, J., Molyneaux, A., Favrat, D., Maréchal, F., Zehnder, M., and Godat, J., 2002, "Compresseur radial pour pompe à chaleur biétagée, phase 1," OFEN Technical Report No. 220195, Swiss Federal Office for Energy.
5. Agrawal, G. L., 1997, "Foil Air/Gas Bearing Technology—An Overview," ASME Paper No. 97-GT-347.
6. Walton, I. J. F., and Heshmat, H., 2002, "Application of Foil Bearings to Turbomachinery Including Vertical Operation," ASME J. Eng. Gas Turbines Power, 124(4), pp. 1032–1041.
7. R.T.P. Whipple, Theory of the Spiral Grooved Thrust Bearing with Liquid or Gas Lubricant, Technical Report, Great Britain Atomic Energy Research Establishment, Harwell, Berks, England, 1951.
8. E. A. Muijderman, Spiral Groove Bearings. in Philips research reports: Suppl. Springer-Verlag, 1966.
9. Vohr, J., and Chow, C., 1965, "Characteristics of Herringbone-Grooved, Gas- Lubricated Journal Bearings," ASME J. Basic Eng., 87, pp. 568–578.
10. Malanoski, S. B., 1967, "Experiments on an Ultrastable Gas Journal Bearing" ASME J. Lubr. Technol., 89, pp. 433–438.
11. Cunningham, R., Fleming, D., and Anderson, W., 1971, "Experimental Load Capacity and Power Loss of Herringbone Grooved Gas Lubricated Journal Bearings," ASME J. Lubr. Technol., 93, pp. 415–422.
12. Gu, L., Guenat, E., and Schiffmann, J. (October 30, 2019). "A Review of Grooved Dynamic Gas Bearings." ASME. Appl. Mech. Rev. January 2020; 72(1): 010802.
13. Van der Stegen, R. H. M., "Numerical Modelling of Self-Acting Gas Lubricated Bearings With Experimental Verification," Doctoral thesis, The University of Twente, Enschede, The Netherlands.
14. Reddi, M. M., and Chu, T. Y., 1970, "Finite Element Solution of the Steady- State Compressible Lubrication Problem," ASME J. Lubr. Technol., 92(3), pp. 495–502.
15. Laiyun Song, Kai Cheng, Hui Ding, Shijin Chen, and Qiang Gao, Analysis of static and dynamic characteristics of spiral-grooved gas journal bearings in high speed, Proceedings of the Institution of Mechanical Engineers, Part C: Journal of Mechanical Engineering Science 2019 233:19-20, 6774-6792.
16. Constantinescu, V. N., and Galetuse, S. (July 1, 1992). "On Extending the Narrow Spiral-Groove Theory to Configurations of Interest in Seals." ASME. J. Tribol. July 1992; 114(3): 563–566. https://doi.org/10.1115/1.2920918.
17. Chen, Y., Wang, H., Wang, X. et al. Performance Analysis and Geometrical Design of Spiral-Grooved Thrust Bearing Employing CFD Model. J. Inst. Eng. India Ser. C 102, 765–775 (2021). https://doi.org/10.1007/s40032-021-00689-5.
18. Yang, G., Du, J., Ge, W., Liu, T., and Yang, X. (November 30, 2016). "Dynamic Characteristics of Spiral-Grooved Opposed-Hemisphere Gas Bearings." ASME. J. Tribol. May 2017; 139(3): 031704. https://doi.org/10.1115/1.4034423.
19. Hashimoto, H., and Ochiai, M., 2008, "Optimization of Groove Geometry for Thrust Air Bearing to Maximize Bearing Stiffness," ASME J. Tribol., 130(3), p. 031101.
20. Hashimoto, H., and Namba, T., 2009, "Optimization of Groove Geometry for a Thrust Air Bearing According to Various Objective Functions," ASME J. Tribol., 131(4), p. 041704.
21. Malanoski, S. B., and Pan, C., 1965, "The Static and Dynamic Characteristics of the Spiral-Grooved Thrust Bearing," ASME J. Basic Eng., 87, pp. 547–558.